Evidence of a barrier oxidation dependence on the interfacial magnetism in Co/alumina based magnetic tunnel junctions

N.D. Telling[1], G. van der Laan[1], S. Ladak[2], R.J. Hicken[2] and E. Arenholz[3]

[1]Magnetic Spectroscopy Group, CCLRC Daresbury Laboratory, Warrington WA4 4AD, UK

[2]University of Exeter, Stocker Road, Exeter EX4 4QL, UK

[3]Advanced Light Source, Berkeley, CA 94720, USA

Soft x-ray absorption spectroscopy and magnetic circular dichroism at the Co $L_{2,3}$ edge have been applied to explore the near-interfacial magnetism of Co electrodes in Co/alumina based magnetic tunnel junctions. By taking into account the formation of CoO at the FM/barrier interface, the change in the total magnetic moment on metallic Co atoms as a function of barrier oxidation has been determined. The results demonstrate a strong correlation between the Co moments and measured TMR values, and an enhancement in the Co moments for moderate oxidation times.

72.25.Mk, 75.70.Cn, 78.70.Dm

I. INTRODUCTION

Magnetic tunnel junctions (MTJs) consist of thin insulating barrier layers sandwiched between ferromagnetic layers. The large tunnel magnetoresistance (TMR) found in these structures has led to an intensive investigation of their properties over the last ten years [1,2]. Most recently, there have been some exciting developments with the realisation of a 2-3 fold increase in the values of TMR compared to those previously obtained [3,4], hence making these structures even more promising for applications in areas such as 'spintronics' and magnetic recording. Currently there are several theoretical models proposing alternative suggestions for the mechanisms underlying the spin-polarised tunneling. Whilst models for MTJs consisting of crystalline MgO barriers consider the symmetry of the wavefunctions to be the key factor [5], alternative models for Co/alumina based MTJs suggest that chemical interfacial bonding plays a dominant role [6,7]. These latter models also predict a dependence of the interfacial magnetism on the chemical bonding between ferromagnet and barrier. Thus measurements of the interfacial magnetism can help to assess the validity of these models.

In this study we have utilised soft x-ray absorption spectroscopy (XAS) techniques to probe the near-interface electronic and magnetic structure in operable magnetic tunnel junctions [8], as a function of the barrier oxidation. The use of circularly polarised x-rays enables the element-specific magnetism in 3d transition metals to be probed via measurements of the x-ray magnetic circular dichroism (XMCD) [9]. Previously [8] we found evidence that the net 3*d* spin-polarisation in the ferromagnetic layer in MTJs is dependent upon the ferromagnetic / barrier interface structure. Here we consider the effect of barrier oxidation on the magnetism of metallic Co atoms situated near to the Co/alumina interface.

II. EXPERIMENTAL

Magnetic tunnel junctions with oversized junction areas were prepared using a combination of magnetron sputtering and plasma oxidation as described elsewhere [10]. The sample structure was of the form SiO_2 / $Ni_{81}Fe_{19}$(80Å) / Co(20Å) / Al(20Å+plasma oxidation for *X* seconds) / $Ni_{81}Fe_{19}$(100Å) / Cu(30Å), where the oxidation time *X* varied from 0 to 600s. Current-voltage (I-V) and TMR measurements were obtained from these junctions using a conventional d.c. four-point probe technique. The large junction areas were necessary to obtain sizeable signals for XAS and XMCD measurements. The trend in TMR with oxidation time for this series was found to be similar to other reports [11,12].

XAS and XMCD measurements at the Co $L_{2,3}$ edge were performed on these *operable* MTJs by allowing x-rays to strike an area of the sample containing the lower ferromagnetic electrode structure covered with the alumina barrier (see inset to Fig. 1). Experiments were performed on beamline 4.0.2 at the Advanced Light Source, Lawrence Berkeley National Laboratory, using 98% circularly polarised soft x-rays. Absorption spectra were obtained in total-electron-yield mode by measuring the drain current via the lower electrodes. This method enhances the sensitivity to the Co/alumina interface owing to the limited electron-escape depth. Additionally, by limiting the thickness of the Co layer directly beneath the alumina to 20Å, the interface region comprises a greater proportion of the measured volume. The XMCD was obtained by fixing the helicity of the incident light and measuring the difference in absorption upon reversing the magnetisation of the Co layer using an externally applied field.

III. RESULTS AND DISCUSSION

Co $L_{2,3}$ x-ray absorption spectra obtained as a function of barrier oxidation time, are shown in Figs 1(a) and (b). As in our previous study [8], the gradual formation of CoO in the Co layer can be witnessed by the appearance of the CoO multiplet structure (indicated by the arrows) superimposed on the metallic Co spectrum. Hence the absorption spectra can be considered as composite curves consisting of a linear superposition of the absorption curves from the metallic Co portion and the CoO region. However, as we found previously [8], there is no contribution to the XMCD spectra (shown in Fig. 1(c)) from the CoO regions. This is consistent with the paramagnetic nature of these regions at room temperature, and the formation of such regions has been used to explain the drop in TMR with increased barrier oxidation due to spin-flip scattering in the oxide [12].

In order to extract the magnetic moment of the unoxidised (i.e. metallic) portion of the Co layer, it is necessary to determine the normalisation of the composite magnetisation-averaged absorption curve. To do this we performed a non-linear least squares analysis on the composite curve by fitting three components: (1) a metallic Co absorption curve representing transitions to the unoccupied 3d states only, (2) a background function with a 2:1 step ratio at the L_3 and L_2 thresholds, approximating transitions to s- and continuum states, and (3) a CoO absorption curve obtained from a reference standard [13]. A typical example of the curves used for the fitting are shown in Fig. 2. The first curve was obtained from the absorption spectrum for the underoxidised MTJ (0s barrier oxidation time), following subtraction of the step-like function. The number of 3d holes is proportional to the background-subtracted integrated absorption spectrum [14]. In the fitting procedure we fixed the

scaling of the step-like function (curve 2) from 0 in the pre-edge region, to 1 in the post L_2 absorption edge region (outside the range visible in the figure), and used the scaling of the metallic Co curve as a fitting parameter. In this way we could allow for variation between samples in the number of 3d holes in the metallic Co portion. Such a variation is the result of charge transfer at the Co/alumina interface.

The other fitting parameters used were the scaling of the CoO curve and the scaling of the composite curve. The relative energy shift between the CoO and metallic Co curves was found by varying this parameter and obtaining a best-fit value for the entire sample series. The fits were improved by convoluting the CoO spectrum with a Gaussian line shape (σ=0.2 eV) to account for differences in the energy resolution between our measured data and the CoO reference data.

Following the normalisation procedure discussed above, and with additional corrections made for the sample geometry and the degree of circularly polarised light, the total magnetic moment per metallic Co atom was calculated using the well-known sum rules for the orbital, m_L, and spin moment, m_S (neglecting the magnetic dipole term) [9]:

$$m_L = -\frac{4}{3}\frac{\Delta A_3 + \Delta A_2}{A_3 + A_2} n_h \quad ; \quad m_S = -2\frac{\Delta A_3 - 2\Delta A_2}{A_3 + A_2} n_h$$

where $\Delta A_{2,3}$ and $A_{2,3}$ are the integrated intensities of the difference (XMCD) and magnetisation-averaged absorption curves, respectively, over the Co $L_{2,3}$ edges, and n_h is the number of 3*d* holes which is proportional to $A_3 + A_2$ [14]. Given that n_h is unknown for a given sample with barrier oxidation time, *X*, we determine here instead the moment relative to the underoxidised (0s barrier oxidation time) sample by replacing n_h with the scaling factor $\left(A_3 + A_2\right)_X / \left(A_3 + A_2\right)_0$. The total magnetic moment ($m_T = m_L + m_S$) thus calculated is shown versus barrier oxidation time in Fig. 3. Here the

value of m_T for the 0s barrier oxidation time sample has been arbitrarily scaled to unity. The corresponding TMR measured is also shown in the figure.

From Fig. 3 it is clear that the Co moment in the unoxidised region is closely connected to the TMR and increases with barrier oxidation time, peaking at values that correspond to the optimum TMR. Recent theoretical calculations using a Green's function technique [6,7] predict a chemical bonding dependence of the interface magnetic moments in Co/alumina MTJs. For an Al-terminated Co/alumina interface, the moment on the Co atoms closest to the interface drops to 1.15 μ_B (compared to a bulk value of 1.68 μ_B). However, the interface moment is close to the bulk value for an O-terminated interface in which the Al bonds are saturated. The calculations also show that further O addition to this interface is adsorbed on the Co surface and creates an O-terminated interface with a lower average moment of 1.5 μ_B per Co interface atom [7]. The moments shown in Fig. 3 reveal an initial increase for moderate oxidation times followed by a decrease for lengthy oxidation times. This trend is consistent with the theoretical moments [6,7], given that we would expect the amount of oxygen available at the interface to increase with barrier oxidation time. Hence the changes in Co moment can be attributed to an initial change from an Al-terminated interface in the underoxidised state, to an O-terminated interface for intermediate oxidation times. Further increases in the oxidation time then provide excess O atoms that are adsorbed on the Co surface resulting in a reduction in the average Co moment.

In addition to the changes in interface moments, the calculations [6,7] also indicate that positive spin-polarised tunneling occurs via specific O atoms in the highest oxygen content interface. Thus it might be expected that the TMR would be largest for the longest barrier oxidation times. However, our x-ray absorption measurements show that the amount of CoO increases with oxidation time. This

would tend to reduce the TMR due to spin-flip scattering in the CoO, and hence could dwarf changes in the spin-polarised tunneling caused by O adsorbed by the Co surface.

IV. CONCLUSION

Soft x-ray absorption techniques have been used to extract the total magnetic moment on Co atoms near the Co/alumina interface in magnetic tunnel junctions. It was found that these near-interface moments are closely correlated with the measured TMR, and follow a trend that is consistent with a theoretical model [6,7] that includes the effects of chemical interface bonding. We further note that an enhanced magnetisation of the Co atoms that coincides with the optimum TMR has also been observed recently for $Co_{70}Fe_{30}$/Alumina [15]. Thus it would appear that chemical bonding plays a key role in determining the interfacial magnetism and spin-polarised tunneling in Co/alumina based magnetic tunnel junctions.

ACKNOWLEDGEMENT

The Advanced Light Source is supported by the Director, Office of Science, Office of Basic Energy Sciences, of the U.S. Department of Energy under Contract No. DE-AC02-05CH11231.

References

1. J S Moodera, L R Kinder, T M Wong, and R Meservey, Phys. Rev. Lett. **74**, 3273 (1995).
2. E Y Tsymbal, O N Mryasov and P R LeClair, J. Phys.: Condens. Matter **15**, R109 (2003).
3. S S P Parkin, C Kaiser, A Panchula, P M Rice, B Hughes, M Samant and S E Yang, Nat. Mat. **3**, 862 (2004).
4. S Yuasa, T Nagahama, A Fukushima, Y Suzuki and K Ando, Nat. Mat. **3**, 868 (2004).
5. X –G Zhang and W H Butler, Phys. Rev. B **70**, 172407 (2004).
6. I I Oleinik, E Y Tsymbal, and D G Pettifor, Phys. Rev. B **62**, 3952 (2000).
7. K D Belashchenko, E Y Tsymbal, I I Oleynik, and M van Schilfgaarde Phys. Rev. B **71**, 224422 (2005) .
8. N D Telling, G van der Laan, S Ladak and R J Hicken, Appl. Phys. Lett. **85**, 3803 (2004).
9. C T Chen, Y U Idzerda, H -J Lin, N V Smith, G Meigs, E Chaban, G H Ho, E Pellegrin, and F Sette, Phys. Rev. Lett. **75**, 152 (1995); B T Thole, P Carra, F Sette and G van der Laan, Phys. Rev. Lett. **68**, 1943 (1992).
10. N D Hughes and R J Hicken, J. Phys. D: Appl. Phys. **35**, 3153 (2002).
11. J J Sun, V Soares and P P Freitas, Appl. Phys. Lett. **74**, 448 (1999).
12. J S Moodera, E F Gallagher, K Robinson and J Nowak, Appl. Phys. Lett. **70**, 3050 (1997).
13. T J Regan, H Ohldag, C Stamm, F Nolting, J Lüning, J Stöhr, and R L White, Phys. Rev. B **64**, 214422 (2001).
14. B T Thole and G van der Laan, Phys. Rev. A **38**, 1943 (1988).

15. J Schmalhorst, M Sacher, A Thomas, H Brückl, G Reiss and K Starke, J. Appl. Phys. 97, 123711 (2005).

Figure Captions

Fig 1: X-ray absorption spectra measured across the Co L_3 absorption edge for the two saturation magnetization directions (symbols and solid lines), for barrier oxidation times of (a) 0s and (b). The difference spectra (XMCD) for the 0s and 360s sample are shown in (c). The inset shows the sample geometry used.

Fig. 2: Magnetisation-averaged x-ray absorption spectrum measured from the 360s barrier oxidation sample (open circles) and best-fit model (solid line), using a superposition of the curves labelled 1-3, details of which are given in the text.

Fig. 3: Relative Co moment determined by XMCD as a function of barrier oxidation time following the fitting and normalisation procedure described in the text. The measured TMR values are also given. Drawn lines are guides to the eye.

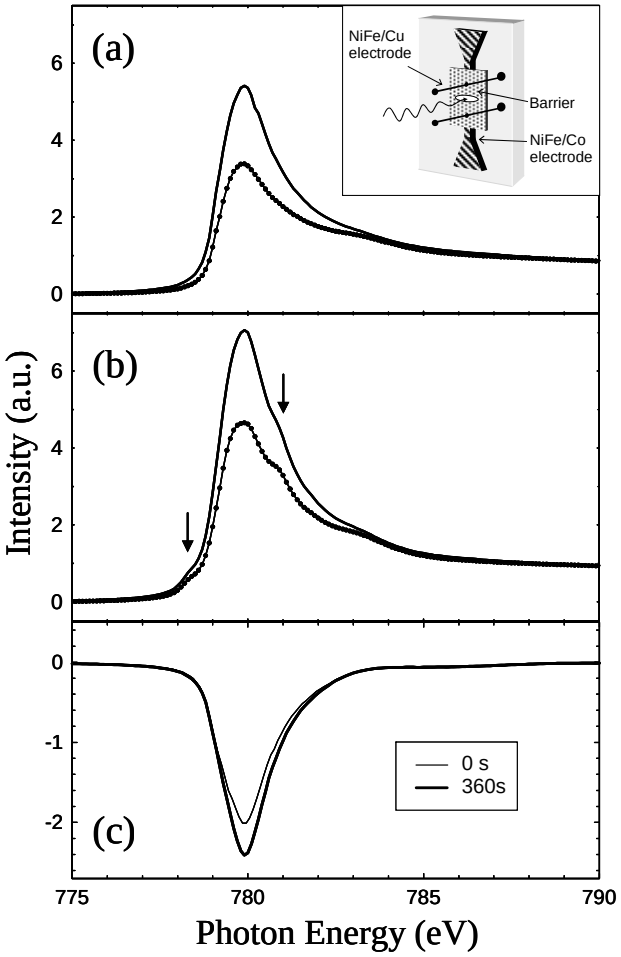
(a)
(b)
(c)
NiFe/Cu electrode
Barrier
NiFe/Co electrode
0 s
360s
Intensity (a.u.)
Photon Energy (eV)
775
780
785
790

Figure 1

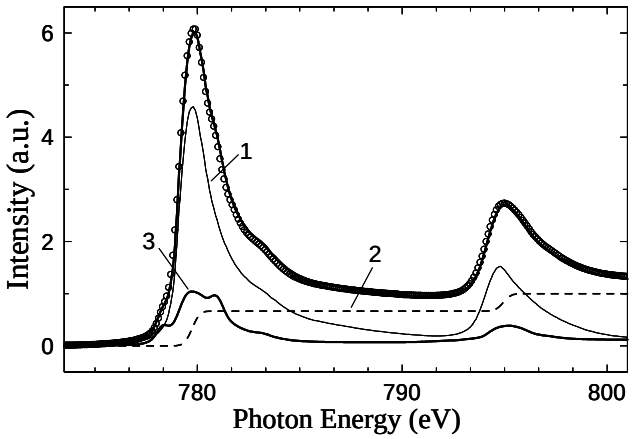

Figure 2

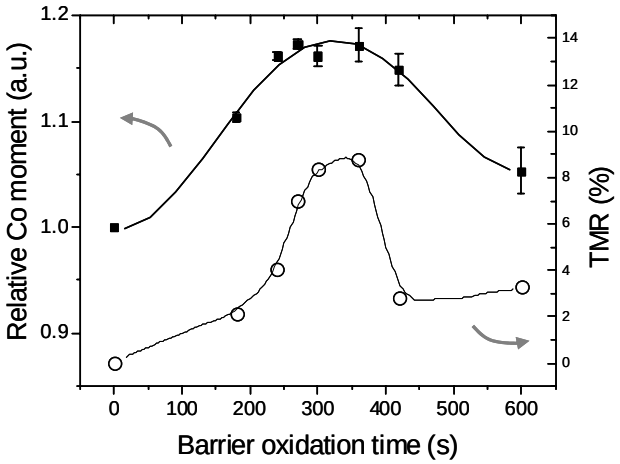
Relative Co moment (a.u.)
TMR (%)
Barrier oxidation time (s)
1.2
1.1
1.0
0.9
14
12
10
8
6
4
2
0
0
100
200
300
400
500
600

Figure 3